Estimating soil moisture content in apple orchards using UAV remote sensing data: Application of LST/LAI two-stage feature space theory

Long Zhao[1,2], Xincheng Lei[2], Yuehua Ding[2], Ningbo Cui[1*], Dan Meng[3*], Yi Shi[4], Minglei Zhang[4], Xinbo Zhao[4], Xiaoxian Zhang[5]

(1. *College of Water Resource and Hydropower, State Key Lab of Hydraulics and Mountain River Engineering, Sichuan University, Chengdu 610065, China*;
2. *College of Horticulture and Plant Protection, Henan University of Science and Technology, Luoyang 471000, Henan, China*;
3. *Chinese Society of Agricultural Engineering, Beijing 100125, China*;
4. *College of Agricultural Equipment Engineering, Henan University of Science and Technology, Luoyang 471023, Henan, China*;
5. *Department of Sustainable Agriculture Sciences, Rothamsted Research, Harpenden, Hertfordshire AL5 2JQ, UK*)

Abstract: Soil moisture is a critical component of the soil-plant-atmosphere continuum (SPAC) in fruit trees. However, high-precision monitoring of orchard soil moisture at the regional scale still remains a challenge. This study presents a two-stage feature space model to estimate root zone soil moisture using UAV remote sensing data. The results indicate that the temperature-leaf area index (TLDI) is negatively correlated with soil water content. The upper triangular space performs highly effectively for deep soil moisture inversion, with R^2 values ranging from 0.56 to 0.66, RMSE between 0.20 and 0.27, and RPD from 1.25 to 1.50. Conversely, the lower triangular space yields superior results for shallow soil moisture inversion, with R^2 values between 0.67 and 0.82, RMSE from 0.15 to 0.19, and RPD between 1.67 and 2.09. The results suggest that the lower triangular space is optimal for shallow soil moisture inversion, while the upper triangular space is more suited for deep soil moisture inversion. This study presents a novel approach for estimating deep soil moisture in orchards, providing a theoretical basis for improving soil moisture management.

Keywords: soil moisture, remote sensing, UAV, LST/LAI, two-stage feature space
DOI: 10.25165/j.ijabe.20251804.9730

Citation: Zhao L, Lei X C, Ding Y H, Cui N B, Meng D, Shi Y, et al. Estimating soil moisture content in apple orchards using UAV remote sensing data: Application of LST/LAI two-stage feature space theory. Int J Agric & Biol Eng, 2025; 18(4): 239–247.

1 Introduction

Soil moisture is a critical variable in the SPAC for fruit tree production. It can impact the physiological and ecological processes of fruit trees, such as transpiration, photosynthesis, nutrient uptake, and fruit formation[1]. Accurate monitoring of soil moisture improves yield prediction and irrigation efficiency, providing a scientific foundation for optimizing regional water resources. However, accurately monitoring the spatial heterogeneity and dynamic changes in deep soil moisture remains a challenge in agricultural remote sensing research due to the complexities introduced by climatic conditions, soil types, and crop growth stages[2]. This challenge is particularly pronounced in deep root zones, where traditional monitoring methods face limitations in data coverage and inversion accuracy.

Traditional monitoring strategies, such as tensiometers, provide high accuracy but are constrained by small sample coverage and low sampling frequency. They are unsuitable for large-scale or real-time monitoring. In contrast, remote sensing technology presents a promising alternative due to its ability to cover large areas and provide high spatial resolution[3]. Despite these advantages, remote sensing models relying on land surface temperature (LST) and vegetation indices (VIs) struggle to accurately estimate soil moisture in deeper layers. This issue is particularly challenging in orchards with heterogeneous vegetation cover and soil properties. VIs tend to saturate under high vegetation density, diminishing their sensitivity to soil moisture variations, while LST models are generally influenced by diurnal temperature fluctuations and surface heterogeneity[4], leading to inconsistent subsurface moisture estimation.

In order to tackle these issues, remote sensing feature space models, including the triangular and trapezoidal LST-fractional vegetation cover (LST-FVC) models, have been developed. The triangular feature space model posits that the dry edge corresponds to the zero-evaporation isoline, and the wet one represents the saturated evaporation isoline[5]. Conversely, the trapezoidal feature space model assumes that soil evaporation and vegetation transpiration change in complete synchrony. However, both

Received date: 2025-02-12 **Accepted date:** 2025-06-22
Biographies: **Long Zhao**, PhD, Associate Professor, research interest: agricultural informatization, Smart agriculture, Email: hkdzhaolong@163.com; **Xincheng Lei**, MS candidate, research interest: agricultural informatization, Email: 240320191178@stu.huast.edu.cn; **Yuehua Ding**, MS, research interest: agricultural informatization, Email: 9943528@huast.edu.cn; **Yi Shi**, PhD, research interest: agricultural informatization, Smart irrigation, Email: shiyigongteng@163.com; **Minglei Zhang**, MS candidate, research interest: agricultural informatization, Email: 15537962990@163.com; **Xinbo Zhao**, PhD candidate, research interest: agricultural informatization, Smart agriculture, Email: 2023201129@stu.njau.edu.cn; **Xiaoxian Zhang**, PhD, research interest: agricultural informatization, Smart agriculture, Email: Xiaoxian.zhang@rothamsted.ac.uk.

***Corresponding author: Ningbo Cui**, Professor, research interest: agricultural informatization, Smart irrigation. NO.24 South section 1 Ring road 1 Wuhou District in Chengdu, Email: cuiningbo@126.com; **Dan Meng**, MS, Engineer, research interest: agricultural informatization. Chinese Society of Agricultural Engineering, Beijing 100125, China, Email: mengd202502@163.com.

approaches face practical limitations. Neither sufficiently considers the varying response times and sensitivities of vegetation and bare soil radiation temperatures to variations in soil moisture[6]. Consequently, they fail to accurately capture the mechanisms underlying the transition of the LST-FVC feature space from a triangular to a trapezoidal configuration, ultimately undermining the accuracy of soil moisture inversion[7].

Aiming to address these shortcomings[8], Sun Hao et al. proposed the two-stage feature space model[9], which comprehensively accounts for the dynamic responses of vegetation and bare soil radiation temperatures. This model elucidates the intrinsic mechanism of the LST-FVC feature space shift. The trapezoidal feature space has been proven to be a theoretical construct arising from the improved sensitivity of bare soil LST to soil moisture compared to that of vegetation LST. When soil moisture is insufficient to notably affect vegetation temperature, the LST-FVC feature space takes the shape of a triangle. However, as soil moisture further decreases and begins to influence vegetation temperature, the feature space gradually transitions from triangular to trapezoidal.

Traditional Normalized Difference Vegetation Index (NDVI)-based feature space models are prone to saturation in areas with dense vegetation, reducing their sensitivity to soil moisture variations[10]. Saturation occurs as NDVI reaches its maximum, challenging the differentiation of soil moisture changes. This study proposed replacing NDVI with leaf area index (LAI), a more reliable indicator of vegetation density and photosynthetic activity, in combination with LST. Based on this, a two-stage trapezoidal feature space model was constructed to enhance soil moisture retrieval at various depths.

Unlike NDVI, which saturates in dense vegetation[11], LAI maintains a linear relationship with vegetation cover and more accurately reflects photosynthetic capacity. LAI is less susceptible to saturation and exhibits a stronger correlation with deep soil moisture. By incorporating LAI, the two-stage trapezoidal feature space model addresses the saturation issue of NDVI and offers a more accurate representation of vegetation's influence on soil moisture. The model divides the feature space into upper and lower triangular regions, facilitating a clearer differentiation between shallow and deep soil moisture response mechanisms while effectively capturing the dynamic characteristics of vegetation and bare soil temperatures.

The objectives of this study include: 1) utilize UAV-based multispectral and thermal infrared imaging technology to capture high-resolution remote sensing data and monitor dynamic conditions in the orchard; 2) validate the soil moisture inversion model using ground truth data and apply the two-stage trapezoidal feature space model to differentiate shallow and deep soil moisture responses; 3) replace NDVI with LAI to enhance model accuracy and integrate LAI with LST to improve deep soil moisture inversion; and 4) develop the TLDI model to enhance soil moisture estimation accuracy.

2 Materials and methods

2.1 Study area

The study was conducted in an apple orchard located in Fufeng County, Baoji City, Shaanxi Province, within the Weihe Basin of the Guanzhong Plain. The region covers an area of 720 km^2 and experiences a continental humid monsoon climate characterized by an annual average temperature of 12.4°C, 592 mm of rainfall, and a frost-free period of 209 d. The 40.2 hm^2 orchard cultivates the 'Gala' variety of apple trees, planted at a spacing of 1.0 m×3.5 m. The soil consists of a mixture of sand, loam, and clay, exhibiting critical properties such as bulk density, porosity, and hydraulic conductivity. These properties significantly influence water retention and movement. Nutrient availability is governed by factors like soil pH, electrical conductivity, and organic matter content. These features are essential for accurate soil moisture inversion, precision agriculture, and water resource management (Figure 1).

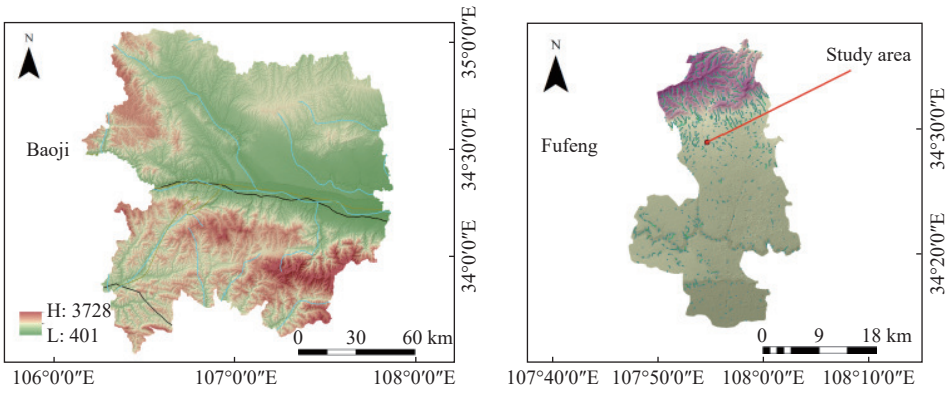

Figure 1 Location of the study area

2.2 Data sources

2.2.1 UAV platform specifications and onboard sensors

The experiment was conducted on April 10 and May 6, 2023. A DJI M30ORTK drone equipped with thermal infrared and multispectral sensors from MicaSense (USA) was utilized to capture data. Flights were carried out at an altitude of 80 meters and a speed of 5 m/s, with 80% forward and side overlap. The data were collected between 14:00 and 15:00 local time under clear skies and stable lighting, without cirrus or cumulonimbus clouds, ensuring high-quality imagery. The drone data facilitated the calculation of LAI from NDVI images and the determination of LST via reflectance maps generated using Pix4Dmapper after stitching, calibration, and preprocessing of the thermal infrared images.

2.2.2 Soil moisture content

The traditional drying method was used to determine soil water content (SWC) across a 70 m×80 m orchard area with 27 sampling points. Samples were taken from depths of 0 cm-60 cm, sealed to prevent moisture loss, and dried at 105°C±2°C until they reached a constant dry weight. The process was validated by rehydrating and redrying the samples, with all equipment calibrated to ensure accuracy. The SWC was determined using the following formula:

$$\mathrm{SWC}(\%) = \frac{M_{\mathrm{wet}} - M_{\mathrm{dry}}}{M_{\mathrm{dry}}} \times 100 \quad (1)$$

where, M_{wet} is the wet weight; M_{dry} is the dry weight.

2.2.3 LAI data

A fisheye camera (180° wide-angle lens) was adopted to capture images of apple tree leaves from the ground at 27 locations within the orchard. For each location, three images of the same tree were taken and processed using Plant Canopy Analysis System (PCAS) software. The average of these images was used to calculate the LAI for each tree.

2.3 Remote sensing data

Pix4Dmapper software was employed to stitch the drone-captured images, followed by radiometric and geometric corrections to minimize distortions. Pseudo-invariant feature radiometric correction, using strategically placed whiteboard images, was applied to generate accurate surface reflectance images. Subsequently, ENVI 5.6 software was utilized to crop the experimental area, classify the apple trees, and extract their spectral images using the BandMath tool.

2.4 NDVI calculation and calibration

Vegetation indices are typically associated with the abundance of green vegetation and serve as quantitative measures for assessing vegetation cover. Over the years, various vegetation indices have been developed to interpret remote sensing data, with the NDVI being the most commonly used. The NDVI can be obtained using the following formula:

$$\mathrm{NDVI} = \frac{\rho_{\mathrm{NIR}} - \rho_{\mathrm{red}}}{\rho_{\mathrm{NIR}} + \rho_{\mathrm{red}}} \tag{2}$$

where, ρ_{NIR} and ρ_{red} represent the surface reflectance in the near-infrared and red bands, respectively.

2.5 TLDI calculation and calibration

This study established a two-stage trapezoidal feature space model leveraging drone-based remote sensing data. The model integrated LST and LAI to estimate soil moisture. The feature space was partitioned into upper and lower triangular regions, where the dry edge represents minimum soil moisture and the wet edge corresponds to maximum soil moisture. Figure 2 illustrates the partitioning of the feature space. The upper triangular region demonstrates greater accuracy for deep soil moisture inversion (40 cm-60 cm), while the lower triangular region is more suitable for shallow soil moisture inversion (0 cm-30 cm). The proposed TLDI exhibits a negative correlation with soil moisture and enhances inversion accuracy, thus improving irrigation precision and water resource management.

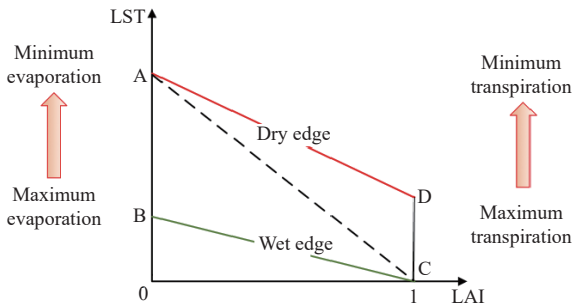

Figure 2 Diagram of the dry and wet edges in land surface temperature and fractional leaf area index (LST/LAI) space

TLDI can be expressed as follows:

$$\mathrm{TLDI} = \frac{T_i - T_{i,\min}}{T_{i,\max} - T_{i,\min}} \tag{3}$$

where, T_i represents the land surface temperature of any given pixel, and $T_{i,\max}$ and $T_{i,\min}$ denote the maximum and minimum land surface temperatures corresponding to respective LAI values. The linear fitting equation for the scatter plot with a given LAI value is referred to as the dry/wet edge equation. The values of $T_{i,\max}$ and $T_{i,\min}$ can be derived from the following equation:

$$T_{i,\max} = a_1 + b_1 \times \mathrm{LAI} \tag{4}$$

$$T_{i,\min} = a_1 + b_1 \times \mathrm{LAI} \tag{5}$$

where, a_1, a_2, b_1, and b_2 represent fitting coefficients. LAI and LST data were extracted and fitted using MATLAB. Then, a scatter plot was generated to approximate the four fitting coefficients.

2.6 Evaluation indicators

This study employed the coefficient of determination (R^2), root mean square error (RMSE), and relative analytical error (RPD) as primary evaluation metrics. R^2 reflects the goodness of fit of the model to the data, with higher values (closer to 1) indicating better model performance. RMSE quantifies the average deviation between predicted and actual values, where lower values denote higher predictive accuracy. RPD assesses the predictive capability of the model, which is defined as the ratio of the sample standard deviation to the standard deviation of the residuals[12]. An RPD greater than 2.0 represents high predictive accuracy[13]; an RPD less than 1.4 indicates general predictive performance; an RPD that falls between 1.4 and 2.0 suggests acceptable predictive accuracy. To eliminate scale differences between data at different depths, this study applies the min-max normalization method for standardization. The data were normalized to account for scale variations across varying depths, ensuring a consistent basis for comparison. R^2, RMSE, and RPD are expressed by Equations (6)-(9):

$$R^2 = 1 - \frac{\sum_{i=1}^{n} (y_i - \hat{y}_i)^2}{\sum_{i=1}^{n} (y_i - \bar{y}_i)^2} \tag{6}$$

$$y' = \frac{y - \min(y)}{\max(y) - \min(y)} \tag{7}$$

$$\mathrm{RMSE} = \sqrt{\frac{\sum_{i=1}^{n} (y_i' - \hat{y}_i')}{n}} \tag{8}$$

$$\mathrm{RPD} = \frac{\sigma_{\mathrm{measured}}}{\sigma_{\mathrm{residual}}} = \frac{\sqrt{\frac{\sum_{i=1}^{n} (y_i' - \bar{y}_i')}{n}}}{\sqrt{\frac{\sum_{i=1}^{n} (y_i' - \hat{y}_i')}{n}}} \tag{9}$$

where, y_i represents the i-th measured value, $\hat{y}_i$ is the i-th predicted value, $\bar{y}_i$ denotes the mean of the measured values, y is the original data, $\min(y)$ is the minimum value of the original data, $\max(y)$ is the maximum value of the original data, y' is the normalized data, and n signifies the number of data points.

3 Results and discussion

3.1 Feature space construction

The NDVI values of 27 locations were obtained using ENVI software and subsequently fitted to the measured LAI values to derive Equation (10) for LAI estimation. LAI data of May 6 can be obtained from NDVI images using Equation (10) without additional measurements.

$$y = 10.616 \times x - 7.72 \quad (10)$$

where, y represents LAI, and x denotes NDVI. Figure 3 shows the NDVI image of the apple trees, and Figure 4 depicts the LAI image of the apple trees on April 10.

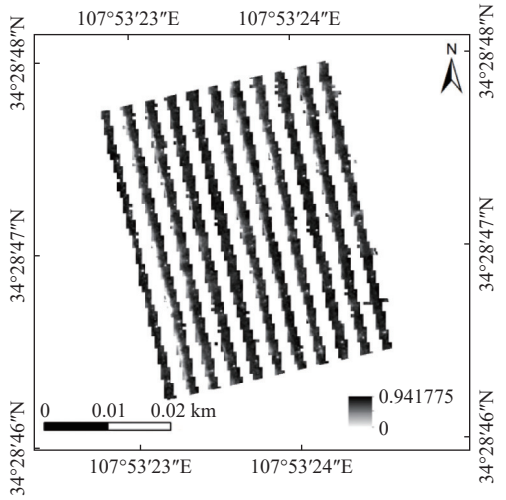

Figure 3 NDVI image of the apple trees

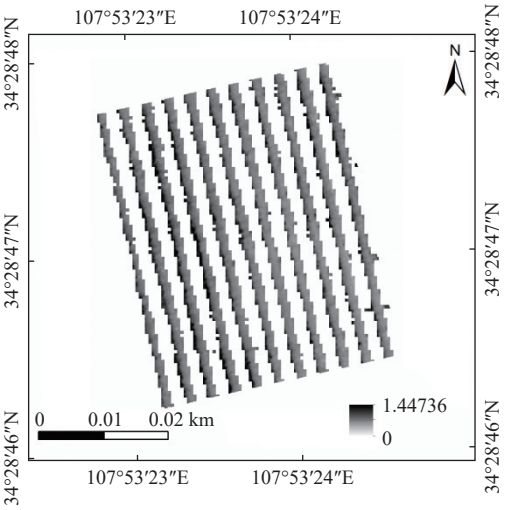

Figure 4 LAI image of the apple trees on April 10

The LST was derived from drone-based thermal infrared images processed using Pix4Dmapper. With an accuracy exceeding 90%, it served as a reliable representation of the actual surface temperature[14], as shown in Figure 5.

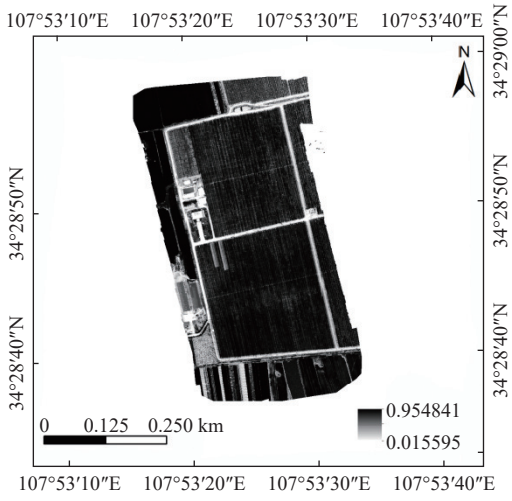

Figure 5 Remote sensing map of the surface temperature

3.2 Feature space distribution

The LST and LAI data were analyzed to obtain the relevant results. The two-stage feature space model was developed to extract the boundary values of LST associated with LAI. Subsequently, linear regression was applied to generate the fitting lines and formulas for the dry and wet edges, providing theoretical support for soil moisture inversion[15].

Table 1 lists the dry and wet edge fitting equations for the two-stage feature space model on April 10 and May 6, 2023. On April 10, the upper triangular dry edge equation yielded an R^2 value of 0.7609, while the lower triangular dry edge equation demonstrated higher accuracy with an R^2 value of 0.8433. The wet edge equations for both triangular spaces did not report R^2 values.

Table 1 Dry and wet edge fitting equations

Date	Fitting equation	R^2
2023-4-10	Upper triangular dry edge: $y = -4.7691x+50.4021$	0.7609
	Upper triangular wet edge: $y = -14.539x+53.6932$	
	Lower triangular dry edge: $y = -14.539x+53.6932$	0.8433
	Lower triangular wet edge: $y = -1.7498x+25.1206$	
2023-5-6	Upper triangular dry edge: $y = -3.7457x+43.4131$	0.4607
	Upper triangular wet edge: $y = -26.585x+45.1363$	
	Lower triangular dry edge: $y = -26.585x+45.1363$	0.6937
	Lower triangular wet edge: $y = -2.6575x+26.4399$	

On May 6, the upper triangular dry edge equation showed an R^2 value of 0.4607, indicating reduced accuracy compared to April 10. By comparison, the lower triangular dry edge equation achieved an R^2 value of 0.6937, representing improved performance. These results suggest that the lower triangular space provides higher fitting accuracy, particularly for dry edges, thus supporting its suitability for soil moisture inversion in specific scenarios[16].

3.3 Soil moisture remote sensing inversion

The TLDI values were obtained from the data of LST and LAI of 27 detection points within the test area[17]. Subsequently, a linear regression method was employed to correlate the measured soil moisture with the parameters of TLDI. The inversion accuracy was derived from the coefficient of determination (R^2). The distribution of 27 detection points for LST and LAI is shown in Figures 6 and 7.

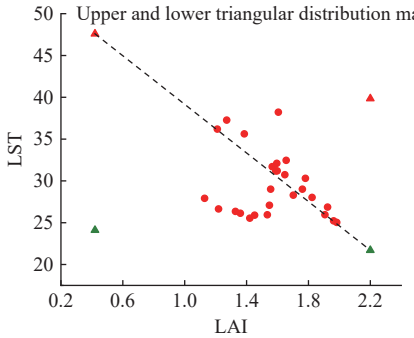

Figure 6 Feature space distribution on April 10

Figures 8 and 9 illustrate the fitting results of TLDI and soil moisture content at depths of 0 cm-60 cm on April 10 and May 6, 2023, respectively. The depth of the shallow soil region was defined as 0 cm-30 cm, while that of the deep soil region was set to be 40 cm-60 cm. TLDI and soil moisture at varying depths displayed a negative correlation, and the coefficient of determination (R^2) decreased with soil depth[18].

According to the results of shallow soil moisture inversion on April 10, the lower triangular space outperformed the upper triangular space across all major metrics, with R^2 values of 0.8180,

0.7801, and 0.7338, RMSE values of 0.1695, 0.1696, and 0.1851, and RPD values of 2.0897, 2.0598, and 1.8602, reflecting high accuracy and predictive reliability. In contrast, the upper triangular space yielded lower R^2 values of 0.7006, 0.6806, and 0.6480, RMSE values of 0.1960, 0.2075, and 0.1970, and RPD values of 1.5011, 1.5379, and 1.5607, suggesting reduced precision in shallow soil moisture inversion[19].

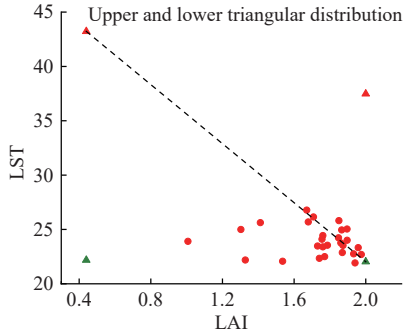

Figure 7 Feature space distribution on May 6

In the deep soil region, the upper triangular space demonstrated higher values of R^2 (0.6395, 0.5750, and 0.5604) and RMSE (0.2259, 0.2037, and 0.2176). Additionally, the upper triangular space achieved greater RPD values of 1.3081, 1.2542, and 1.3498. In contrast, the lower triangular space has R^2 values of 0.6115, 0.5481, and 0.4749, RMSE values of 0.2272, 0.2208, and 0.2817, and RPD values of 1.2923, 1.1605, and 0.8935, further supporting the superior performance of the upper triangular space for deep soil moisture inversion.

In conclusion, the lower triangular space is suitable for shallow soil moisture inversion, while the upper triangular space performs effectively for deep soil moisture inversion[20].

The fitting results of May 6 followed a similar pattern to those observed on April 10. For the shallow soil region, the R^2 values in the upper triangular space were 0.7063, 0.6922, and 0.6625. These values were lower than those in the lower triangular space (0.8054, 0.7299, and 0.6756); the higher the R^2, the better the performance. And the RMSE values in the upper triangular space were 0.2129, 0.2624, and 0.2144, while those in the lower triangular space were lower at 0.1603, 0.1509, and 0.1850; the smaller the RMSE, the better the performance. Meanwhile, the RPD values in the upper triangular space were 1.5727, 1.4553, and 1.1090, lower than those in the lower triangular space (2.0073, 1.7360, and 1.6724); the higher the RPD, the better the performance. These results verify that the lower triangular space provides higher accuracy for shallow soil moisture inversion[21].

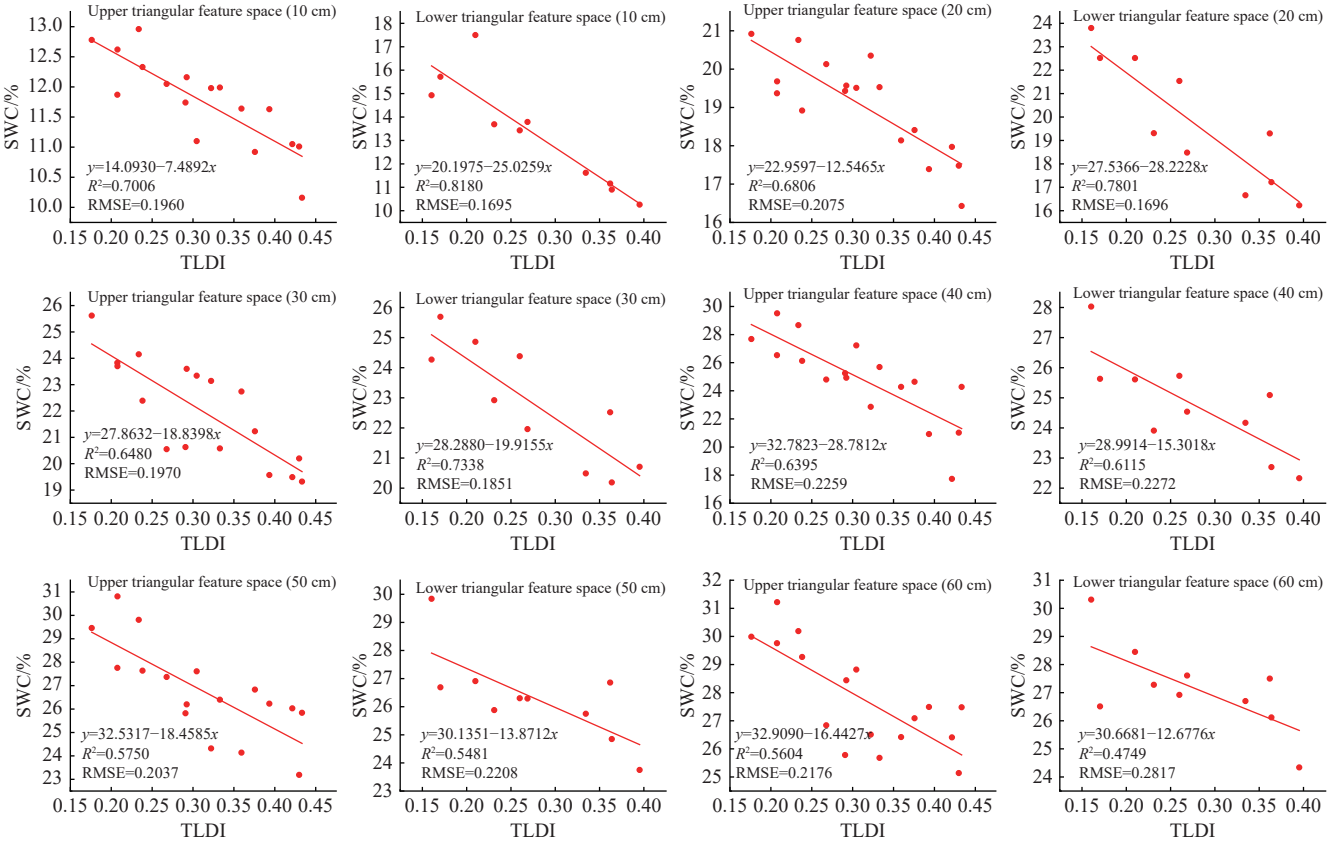

Figure 8 Linear regression of TLDI and SWC/% fitting results for April 10

Regarding the deep soil region, the upper triangular space outperformed the lower triangular space. The R^2 values in the upper triangular space were 0.6606, 0.6273, and 0.5936, higher than those in the lower triangular space, which were 0.5274, 0.4405, and 0.4388. The RMSE values in the upper triangular space were 0.2210, 0.2356, and 0.2717, lower than those in the lower triangular space (0.2252, 0.2534, and 0.2722). The RPD values in the upper triangular space were 1.5001, 1.3362, and 1.3705, greater than those in the lower triangular space, which were 1.4279, 1.2876, and 1.2899.

The results demonstrate that the lower triangular feature space is suitable for shallow soil moisture inversion[22], while the upper triangular feature space achieves satisfying performance for deep soil moisture inversion.

The TLDI, calculated using the dry and wet edges in the LST-LAI two-stage feature space[23], yielded enhanced fitting results for

deep soil moisture within the upper triangular feature space[24]. This index is more appropriate for modeling deep soil moisture. By comparison, the lower triangular space demonstrates higher inversion accuracy for shallow soil moisture, making it more suitable for shallow moisture modeling. Remote sensing inversion presented lower R^2 values in the deep layer than in the shallow layer[25].

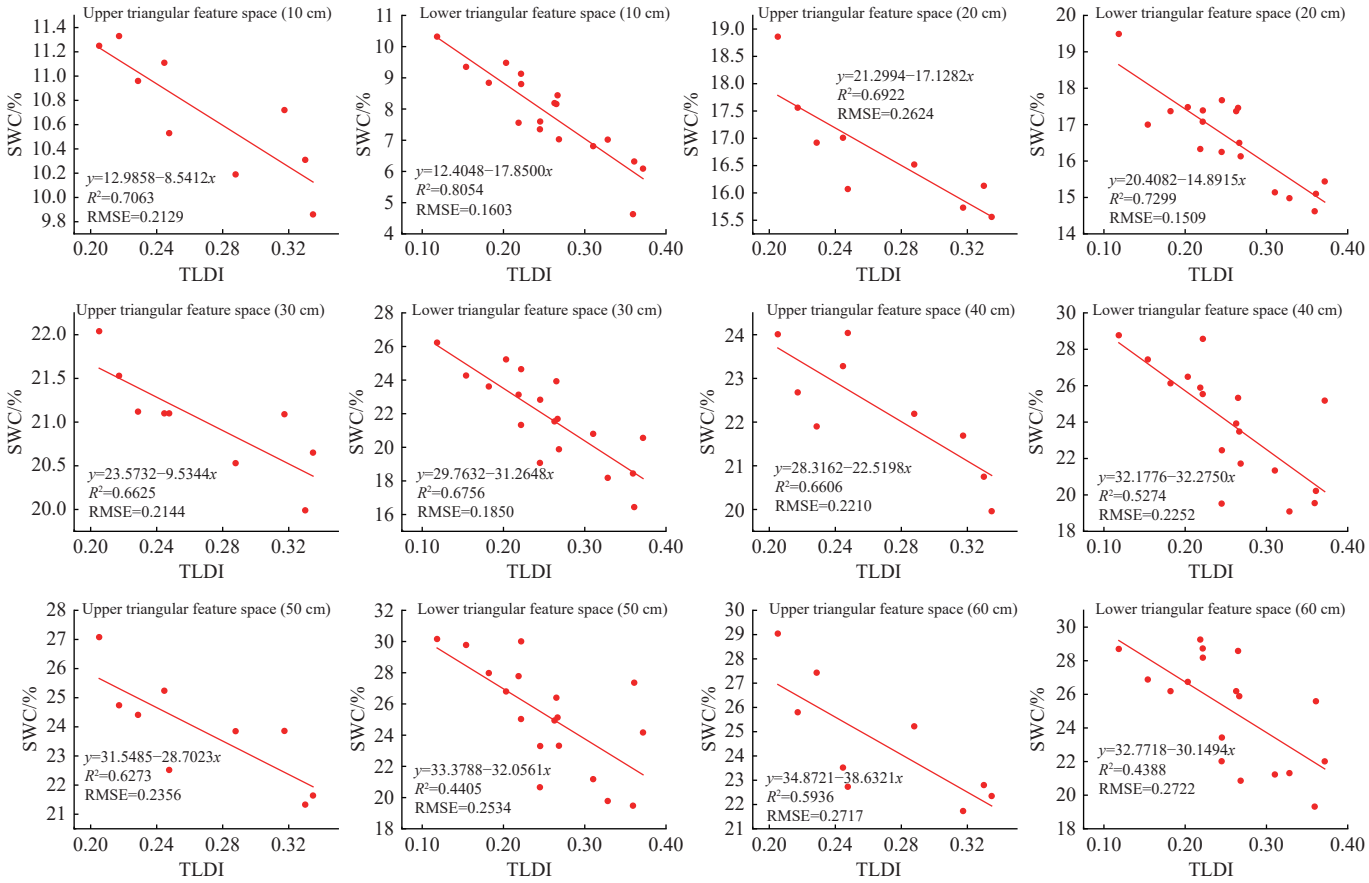

Figure 9 Linear regression of TLDI and SWC/% fitting results for May 6

The results suggest that the upper triangular feature space has superior performance for deep soil moisture inversion, while the lower triangular feature space is optimal for shallow soil moisture inversion, aligning with the evaluation results. Tables 2 and 3 summarize the R^2, RMSE, and RPD values at depths of 0 cm-60 cm for April 10 and May 6.

Table 2 Variation in the upper triangle of the feature space model for R^2, RMSE, and RPD

Date	Evaluation indicator	10 cm	20 cm	30 cm	40 cm	50 cm	60 cm
2023.4.10	R^2	0.7006	0.6806	0.6480	0.6395	0.5750	0.5604
	RMSE	0.1960	0.2075	0.1970	0.2259	0.2037	0.2176
	RPD	1.5011	1.5379	1.5607	1.3081	1.2542	1.3498
2023.5.6	R^2	0.7063	0.6922	0.6625	0.6606	0.6273	0.5936
	RMSE	0.2129	0.2624	0.2144	0.2210	0.2356	0.2717
	RPD	1.5727	1.4553	1.1090	1.5001	1.3362	1.3705

Table 3 Variation in the lower triangle of the feature space model for R^2, RMSE, and RPD

Date	Evaluation indicator	10 cm	20 cm	30 cm	40 cm	50 cm	60 cm
2023.4.10	R^2	0.8180	0.7801	0.7338	0.6115	0.5481	0.4749
	RMSE	0.1695	0.1696	0.1851	0.2272	0.2208	0.2817
	RPD	2.0897	2.0598	1.8602	1.2923	1.1605	0.8935
2023.5.6	R^2	0.8054	0.7299	0.6756	0.5274	0.4405	0.4388
	RMSE	0.1603	0.1509	0.1850	0.2252	0.2534	0.2722
	RPD	2.0073	1.7360	1.6724	1.4279	1.2876	1.2899

3.4 Remote sensing-based soil moisture distribution inversion

The soil moisture content for the shallow layer on April 10 and May 6 was estimated using the fitting function derived from the lower triangular feature space. That for the deep layer was assessed via the fitting function from the upper triangular feature space. Figures 10 and 11 depict the estimated distribution of soil moisture content at depths of 0 cm-60 cm for April 10 and May 6, respectively. Based on these results, the subsequent section presents a detailed evaluation and discussion of the model performance and its applicability.

4 Discussion

4.1 Applicability of the upper triangular feature space in deep soil moisture inversion

Deep soil moisture typically is less susceptible to short-term environmental fluctuations due to the thermal inertia of deep soil. This causes LST to respond more gradually to variations in moisture content. The upper triangular feature space, which integrates LST and LAI, demonstrates high efficiency in capturing changes in deep soil moisture[26]. The upper triangular space integrates LST and LAI to capture the slow response of deep soil moisture to thermal inertia. LST in deep soil is less affected by short-term climatic fluctuations, while LAI reflects long-term root water uptake and photosynthetic dynamics. This physical coupling enables the upper triangular model to better characterize deep soil moisture variations. It possesses high inversion accuracy at depths of 40 cm-60 cm, as evidenced by greater R^2 values (0.6606, 0.6273,

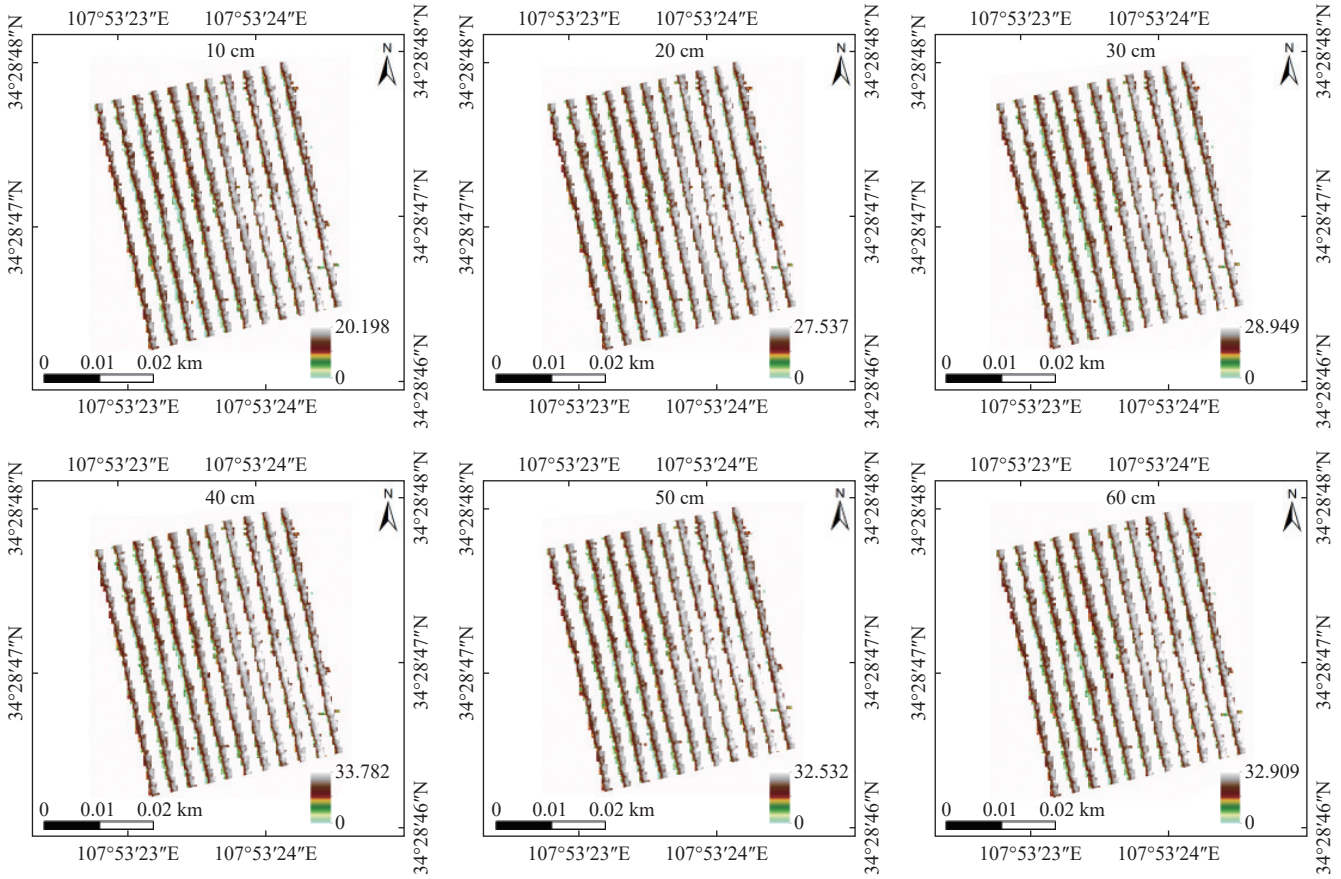

Figure 10 Inversion results of regional soil moisture content in the study area on April 10

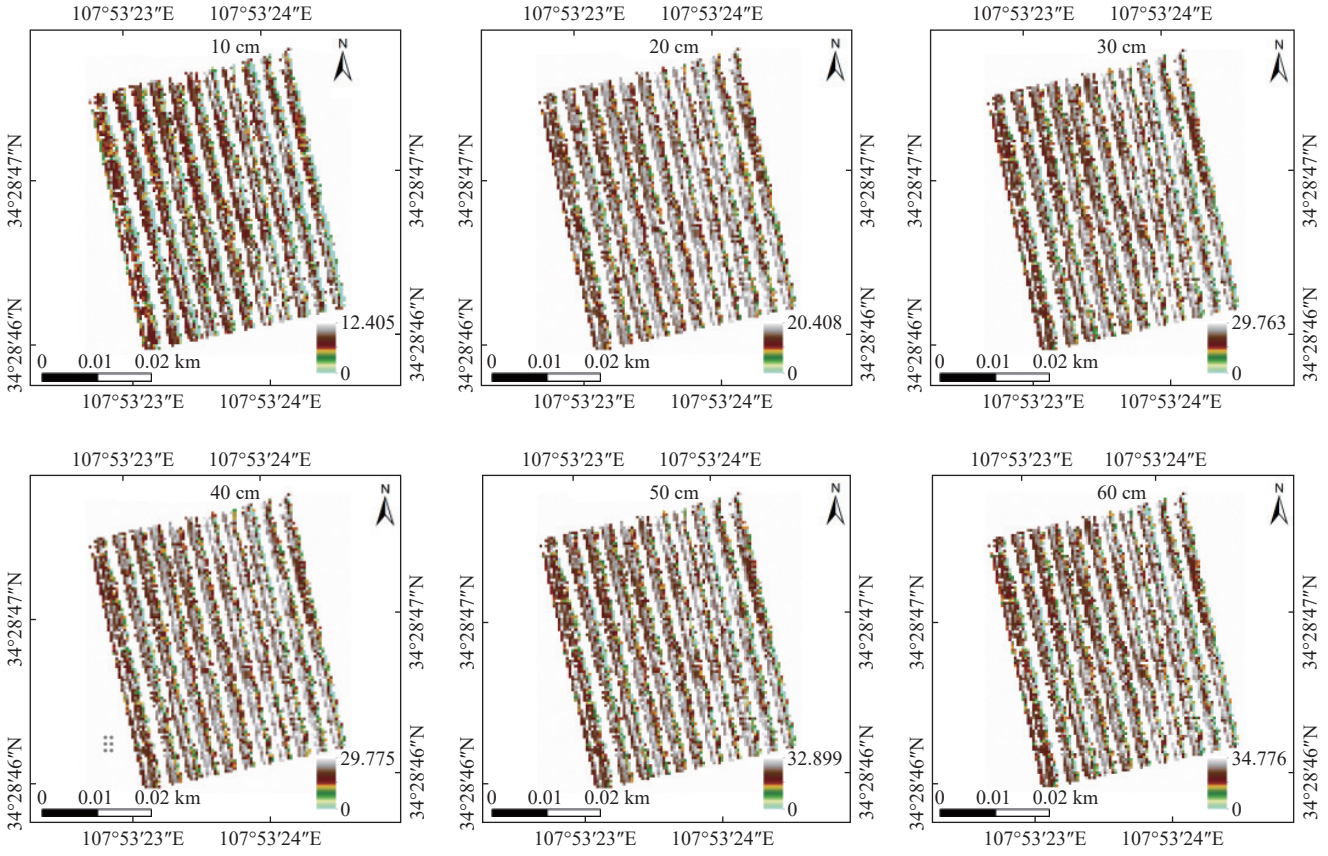

Figure 11 Inversion results of regional soil moisture content in the study area on May 6

and 0.5936) than those of the lower triangular space (0.5274, 0.4405, and 0.4388). These findings suggest that the upper triangular feature space is better suited for modeling gradual variations in deep soil moisture, which is consistent with previous studies.

Additionally, deep soil moisture influences vegetation root

water uptake and photosynthesis. LAI values vary with moisture changes. Due to this, LAI-based feature space models show enhanced performance for deep soil moisture inversion. Given the seasonal and long-term trends in deep soil moisture, combining the upper triangular feature space with time-series analysis provides a robust method for monitoring deep soil moisture via remote sensing, thus contributing to agricultural irrigation optimization and regional water resource management[27].

4.2 Applicability of the lower triangular feature space in shallow soil moisture inversion

Shallow soil moisture is highly sensitive to environmental factors, such as rainfall and evaporation. It can reflect the dynamic balance between water input and output. The lower triangular feature space, by capturing the relationship between LST and LAI, effectively tracks these rapid variations in shallow soil moisture, making it an ideal tool for short-term dynamic monitoring[28]. RMSE evaluation exhibited that the lower triangular feature space outperformed the upper triangular feature space in shallow soil moisture inversion (0 cm-30 cm), with lower RMSE values (0.1603, 0.1509, and 0.1850) than those (0.2129, 0.2624, and 0.2144) in the upper triangular space. Additionally, the RPD values (2.0073, 1.7360, and 1.6724) were higher than those in the upper triangular space (1.5727, 1.4553, and 1.1090). The lower triangular feature space provides more accurate and reliable prediction results for shallow soil moisture inversion, verifying its suitability for monitoring shallow soil moisture. It is highly effective for analyzing rainfall events and managing irrigation. For instance, following a rainfall event, the lower triangular feature space model can accurately capture the rapid wetting of the soil surface layer[29].

Shallow soil moisture impacts vegetation transpiration. When moisture levels are high, enhanced transpiration leads to a reduction in surface temperature. Conversely, under drought conditions, insufficient moisture restricts transpiration. The lower triangular feature space demonstrates high sensitivity to these dynamics, making it particularly effective for soil moisture inversion in regions with dense vegetation coverage[30].

4.3 Limitations of the upper and lower triangular feature space model

Although the upper and lower triangular feature spaces offer distinct advantages for soil moisture inversion at various depths, their complementary nature allows for a more comprehensive solution when used in tandem. The upper triangular feature space excels in deep soil moisture inversion in areas experiencing long-term droughts and dense vegetation. By comparison, the lower triangular feature space is better suited for short-term monitoring of shallow soil moisture. Combining both feature spaces facilitates precise inversion of soil moisture at varying depths, thereby improving precision irrigation and water resource management[31].

Furthermore, the proposed two-stage feature space model surpasses traditional soil moisture inversion models (e.g., NDVI-LST and TVDI models). By substituting LAI for NDVI, the model avoids vegetation saturation issues and promotes the accuracy of deep soil moisture inversion. Compared to machine learning models, ground sensors, and traditional physical models, the proposed model demonstrates greater interpretability, adaptability, and stability. It is well-suited for large-scale and real-time monitoring with reduced computational costs, making it a valuable tool for precision irrigation and other practical applications[32].

Despite its significant applicability in experimental contexts, the two-stage feature space model has limitations in diverse environments. In areas with sparse vegetation or complex soil types, the relationship between LAI and LST can be affected by environmental factors, potentially degrading the model's effectiveness. Additionally, extreme climate events, such as heavy rainfall or abnormal temperatures, can disrupt LST observations and diminish the stability of the dry-wet edge fitting curve[33].

Future research can incorporate multi-source remote sensing data (such as microwave and optical data) and machine learning techniques to expand the model's applicability in complex environments. Additionally, seasonal experiments can be conducted to assess the model's performance during peak vegetation growth and drought periods, thus promoting its generalizability and accuracy.

5 Conclusions

This study employed UAV-based multispectral and thermal infrared imagery to estimate soil moisture in an apple orchard. A two-stage feature space model was developed using the derived LST and LAI data. The results indicated that the TLDI is negatively correlated with soil moisture. The upper triangular feature space is more suitable for estimating deep soil moisture (40 cm-60 cm), with R^2 values of 0.6395 (0.6606), 0.5750 (0.6273), and 0.5604 (0.5936); RMSE values of 0.2259 (0.2210), 0.2037 (0.2356), and 0.2176 (0.2717); and RPD values of 1.3081 (1.5001), 1.2542 (1.3362), and 1.3498 (1.3705). In contrast, the lower triangular space provides better accuracy for shallow soil moisture (0 cm-30 cm), with R^2 values of 0.8180 (0.8054), 0.7801 (0.7299), and 0.7338 (0.6756); RMSE values of 0.1695 (0.1603), 0.1696 (0.1509), and 0.1851 (0.1850); and RPD values of 2.0897 (2.0073), 2.0598 (1.7360), and 1.8602 (1.6724). R^2, RMSE, and RPD values on both April 10 and May 6 revealed that the upper triangular space outperformed in deep soil layers, while the lower triangular space was more effective for shallow layers. Furthermore, soil moisture increased with depth, although the growth trend slowed at greater depths. The results demonstrate the significant potential of soil moisture inversion in the deep layers of orchard soils. The integration of UAV remote sensing technology with the two-stage feature space model (TLDI) improves the accuracy of soil moisture monitoring, particularly for deep soil moisture estimation. This method offers reliable technical support for future soil moisture monitoring. However, several limitations remain, including the model's sensitivity to vegetation types, extreme climatic conditions, and limited temporal sampling. Future research may integrate multi-source data and apply machine learning techniques to improve the model's robustness and generalizability.

Acknowledgements

This work was financially supported by the National Natural Science Foundation of China (Grant No. 52309050), Key R&D and Promotion Projects in Henan Province (Science and Technology Development) (Grant No. 232102110264), Key Scientific Research Projects of Colleges and Universities in Henan Province (Grant No. 24B416001), Youth Backbone Teacher Project of Henan University of Science and Technology (Grants No. 13450013 and 13450010), and Sichuan Province Science and Technology Support Projects (Grants No. 2023YFQ0025, 2024YFHZ0217, 2024ZHCG0101, and 2024YFHZ0200).

[References]

[1] Reich P B, Sendall K M, Stefanski A, Rich R L, Hobbie S E, Montgomery R A. Effects of climate warming on photosynthesis in boreal tree species depend on soil moisture. Nature, 2018; 562: 263–267.

[2] Seneviratne S I, Conti T, Davin E L, Hirschi M, Jaeger E B, Lehner I, et al. Investigating soil moisture–climate interactions in a changing climate: A review. Earth-Science Reviews, 2010; 99(3-4): 125–161.
[3] Araya A, Prasad P V V, Gowda P H, Afewerk A, Abadi B, Foster A J. Modeling irrigation and nitrogen management of wheat in northern Ethiopia. Agricultural Water Management, 2019; 216: 264–272.
[4] Gillies R R, Kustas W P, Humes K S. A verification of the 'triangle' method for obtaining surface soil water content and energy fluxes from remote measurements of the normalized difference vegetation index (NDVI) and surface radiant temperature. International Journal of Remote Sensing, 1997; 18(15): 3145–3166.
[5] Gómez-del-Campo M, Pérez-Expósito M Á, Hammami S B M, Centeno A, Rapoport H F. Effect of varied summer deficit irrigation on components of olive fruit growth and development. Agricultural Water Managemen, 2014; 137: 84–91.
[6] Njoku E G, Entekhabi D. Passive microwave remote sensing of soil moisture. Journal of Hydrology, 1996; 184(1-2): 101–129.
[7] Sandholt I, Rasmussen K, Andersen J. A simple interpretation of the surface temperature/vegetation index space for assessment of surface moisture status. Remote Sensing of Environment, 2002; 79(2-3): 213–224.
[8] Chen S L, Wen Z M, Jiang H, Zhao Q J, Zhang X Y, Chen Y. Temperature vegetation dryness index estimation of soil moisture under different tree species. Sustainability, 2015; 7(9): 11401–11417.
[9] Sun H, Wang Y M, Liu W H, Yuan S Y, Nie R W. Comparison of three theoretical methods for determining dry and wet edges of the LST/FVC space: Revisit of method physics. Remote Sensing, 2017; 9(6): 528.
[10] Li X Y, Jin H G, Ekiundh L, Bouras E H, Olsson P O, Cai Z Z, et al. Estimation of district-level spring barley yield in southern Sweden using multi-source satellite data and random forest approach. International Journal of Applied Earth Observation and Geoinformation, 2024; 134: 104183.
[11] Zhu Z, Li T S, Cui J, Shi X Y, Chen J H, Wang H J. Non-destructive estimation of winter wheat leaf moisture content using near-ground hyperspectral imaging technology. Acta Agriculturae Scandinavica Section B - Soil & Plant Science, 2020; 70(4): 294–306.
[12] Wong T-T. Performance evaluation of classification algorithms by k-fold and leave-one-out cross validation. Pattern Recognition, 2015; 48(9): 2839–2846.
[13] Arias M, Notarnicola C, Campo-Bescós M Á, Arregui L M, Álvarez-Mozos J. Evaluation of soil moisture estimation techniques based on Sentinel-1 observations over wheat fields. Agricultural Water Management, 2023; 287: 108422.
[14] Guo X H, Lei T, Sun X H, Ma J J, Zheng L J, Zhang S W, et al. Modelling soil water dynamics and root water uptake for apple trees under water storage pit irrigation. Int J Agric & Biol Eng, 2019; 12(5): 126–134.
[15] Rudiyanto, Minasny B, Shah R M, Setiawan B I, van Genuchten M T, et al. Simple functions for describing soil water retention and the unsaturated hydraulic conductivity from saturation to complete dryness. Journal of Hydrology, 2020; 588: 125041.
[16] Santos F L M, Rodrigues G, Potes M, Couto F T, Costa M J, Dias S, et al. Moisture content vegetation seasonal variability based on a multiscale remote sensing approach. Remote Sensing, 2024; 16(23): 4434.
[17] Sillero-Medina J A, González-Pérez J, Hueso-González P, González-Fernández J J, Hormaza-Urroz J I, Ruiz-Sinoga J D. Effect of different deficit irrigation regimens on soil moisture, production parameters of mango (*Mangifera indica* L.), and spectral vegetation indices in the mediterranean region of southern spain. Remote Sensing Applications: Society and Environment, 2025; 37: 101415.
[18] Liu Q S, Wu Z J, Cui N B, Zheng S S, Jiang S Z, Wang Z H, et al. Estimating stomatal conductance of citrus orchard based on UAV multi-modal information in Southwest China. Agricultural Water Management, 2025; 307: 109253.
[19] Wang Y X, Yan N N, Zhu W W, Ma Z H, Wu B F. A method to estimate the water storage of on-farm reservoirs by detecting slope gradients based on multi-spectral drone data. Agricultural Water Management, 2025; 307: 109241.
[20] Akinaga T, Saito M, Onodera S, Hyodo F. UAV visual imagery-based evaluation of blue carbon as seagrass beds on a tidal flat scale. Remote Sensing Applications: Society and Environment, 2025; 37: 101430.
[21] Turman A M, Sowby R B, Williams G P, Hansen N C. Remote sensing of residential landscape irrigation in weber county, Utah: Implications for water conservation, image analysis, and drone applications. Sustainability, 2024; 16(21): 9356.
[22] Guo F X, Feng Q, Yang S, Yang W X. Estimation of potato canopy leaf water content in various growth stages using UAV hyperspectral remote sensing and machine learning. Frontiers in Plant Science, 2024; 15: 1458589. doi; 10.3389/FPLS. 2024.1458589.
[23] Fathololoumi S, Vaezi A R, Firozjaei M K, Biswas A. Quantifying the effect of surface heterogeneity on soil moisture across regions and surface characteristic. Journal of Hydrology, 2021; 596: 126132.
[24] Mahasneh H. Drones in agriculture: Real-world applications and impactful case studies. Journal of Natural Science Reviews, 2024; 2(2024): 643–656.
[25] Zhao Y, Wang H X, Song B, Xue P F, Zhang W C, Peth S, et al. Characterizing uncertainty in process-based hydraulic modeling, exemplified in a semiarid Inner Mongolia steppe. Geoderma, 2023; 440: 116713.
[26] Hurlimann A C, Moosavi S, Browne G R. Climate change transformation: A definition and typology to guide decision making in urban environments. Sustainable Cities and Society, 2021; 70: 102890.
[27] Zhang R Z, Nayak A, Houtz D, Watts A, Soltanaghai E, Alipour M. Evaluation of soil moisture retrievals from a portable L-band microwave radiometer. Remote Sensing, 2024; 16(23): 4596.
[28] Escandón-Panchana P, Martinez-cuevas S, Jaya-montalvo M, Herrera-franco G. Review of agricultural cadastre approaches using geomatics for rural development. WIT Transactions on Ecology and the Environment, 2024; 262: 465–478.
[29] Šimůnek J, van Genuchten M T. Modeling nonequilibrium flow and transport processes using HYDRUS. Vadose Zone Journal, 2008; 7(2): 782–797.
[30] Zhao H, Wang J J, Guo J L, Hui X, Wang Y L, Cai D Y, et al. Detecting water stress in winter wheat based on multifeature fusion from UAV remote sensing and stacking ensemble learning method. Remote Sensing, 2024; 16(21): 4100.
[31] Zeng Y J, Su Z B, van der Velde R, Wang L C, Xu K, Wang X, et al. Blending satellite observed, model simulated, and in situ measured soil moisture over Tibetan Plateau. Remote Sensing, 2016; 8(3): 268.
[32] Viscarra Rossel R A, Behrens T. Using data mining to model and interpret soil diffuse reflectance spectra. Geoderma, 2010; 158(1-2): 46–54.
[33] Sun H, Zhang L, Rao Z H, Ji H Y. Determination of moisture content in barley seeds based on hyperspectral imaging technology. Spectroscopy Letters, 2020; 53(10): 751–762.